

Locomotion Mode Transitions: Tackling System- and User-Specific Variability in Lower-Limb Exoskeletons

Andrea Dal Prete^{*1,2}, Zeynep Özge Orhan^{*1,3}, *Student Member, IEEE*,
Anastasia Bolotnikova^{3,4} *IEEE Member, IEEE*, Marta Gandolla²,
Auke Ijspeert³ *Fellow, IEEE*, and Mohamed Bouri^{1,5} *Senior Member, IEEE* .

Abstract—Accurate detection of locomotion transitions, such as walk to sit, to stair ascent, and descent, is crucial to effectively control robotic assistive devices, such as lower-limb exoskeletons, as each locomotion mode requires specific assistance. Variability in collected sensor data introduced by user- or system-specific characteristics makes it challenging to maintain high transition detection accuracy while avoiding latency using non-adaptive classification models. In this study, we identified key factors influencing transition detection performance, including variations in user behavior, and mechanical design of the exoskeletons. To boost the transition detection accuracy, we introduced two methods for adapting a finite-state machine classifier to system- and user-specific variability: a Statistics-Based approach and Bayesian Optimization. Our experimental results demonstrate that both methods remarkably improve detection accuracy across diverse users, achieving up to an 80% increase in certain scenarios compared to the non-personalized threshold method. These findings emphasize the importance of personalization in adaptive control systems, underscoring the potential for enhanced user experience and effectiveness in assistive devices. By incorporating subject- and system-specific data into the model, our approach offers a precise and reliable solution for detecting locomotion transitions, catering to individual user needs, and ultimately improving the performance of assistive devices.

Index Terms—Locomotion mode identification, transition classification, exoskeleton, machine learning

I. INTRODUCTION

Delivering effective assistance during various locomotion activities, such as walking, stair ascent, stair descent, and sitting, is critical for enhancing user experience in lower-limb exoskeletons. Accurate real-time identification of the transitions between different locomotion activities is crucial for developing intelligent systems that deliver seamless and responsive assistance.

A key challenge in real-world exoskeleton applications lies in ensuring adaptability across diverse locomotion tasks.

¹ REHAssist Group, EPFL.

² Department of Mechanical Engineering, Politecnico di Milano.

³ BioRobotics Laboratory (BioRob), EPFL.

⁴ Robotics and InteractionS Team, LAAS-CNRS

⁵ Translational Neural Engineering Laboratory (TNE), EPFL.

(* These two authors contributed equally to this study.

(Corresponding author e-mail: andrea.dalprete@polimi.it)

This article has supplementary downloadable material available at <https://zenodo.org/records/14076104>, provided by the authors. A video from the real-time experiments is available in <https://youtu.be/dxp4wHUmlrA>



Fig. 1: The outdoor environment where the onboard transition detection tests are performed for walk to stair ascent, stair ascent to walk, walk to sit, sit to walk, walk to stair descent, and stair descent to walk transitions

Most control strategies are designed for specific, steady-state activities, like level-ground walking, yet real-world environments demand systems that can handle varied terrains and frequent transitions with dynamic adaptability.

Achieving precise transition detection across different users and conditions is particularly challenging. Variations in user gait, exoskeleton designs, and the need for efficient on-board processing further complicate reliable transition detection between locomotion modes. Most existing methods, often designed for specific locomotion tasks, can fall short when faced with more dynamic, real-world scenarios involving varied terrains and diverse user behaviors.

The finite-state machine (FSM) developed by Cheng et al. [1] offers a structured approach to transition detection, combining different locomotion modes into a single system that leverages key features like hip flexion/extension angle and velocity. In our previous work, we extended this FSM to improve real-time performance on embedded systems,

reducing processing time up to elevenfold with a machine learning-trained threshold method compared to deploying machine learning models directly [2]. This FSM configuration achieved high accuracy with ten healthy subjects across four key locomotion modes: walking, sitting, stair ascent, and stair descent in an outdoor setting presented in Fig. 1.

Testing this method on a different exoskeleton, autonomyo, revealed certain limitations. Unlike eWalk, which features only hip flexion/extension as the active degree of freedom per leg, autonomyo offers three active degrees of freedom, including hip abduction/adduction and knee flexion/extension, making it inherently more complex and heavier. During experiments, eWalk operated in passive mode, benefiting from its lightweight, transparent design, while autonomyo was used in zero-torque mode to maintain transparency. These design differences affected user behavior; with autonomyo, users exhibited slower sitting patterns, smaller pre-sit adjustment steps, and overall more cautious movement.

Moreover, the FSM did not fully accommodate different styles of locomotion due to subject-specific characteristics, such as running-like stair climbing. These findings indicate that while detecting transitions is essential, personalizing this detection to accommodate individual differences can further enhance the efficacy of assistive devices.

In this study we focus on enhancing transition detection algorithms by tailoring them to individual gait patterns and movement characteristics across two distinct exoskeletons. Leveraging real-time experimental data, we introduce two methods, a statistics-based approach and Bayesian optimization to personalize the FSM thresholds, improving detection accuracy by accounting for system- and user-specific variability. Our results demonstrate that these personalized adjustments significantly enhance adaptability and effectiveness, underscoring the potential for responsive, user-centered control in lower-limb exoskeletons and similar assistive devices.

Outline: The rest of the paper is organized as follows. Section II reviews related work, Section III outlines the feature space, finite-state machine, dataset construction, algorithms, and subject and system-specific threshold tuning methods. Section IV presents the conducted human subject experiments. Section V provides the experimental results while a detailed discussion is provided in Section VI, followed by the conclusion in Section VII. Technical details related to the shared dataset are presented in the Supplementary Material.

II. RELATED WORK

A. Locomotion Mode Detection

Locomotion mode identification involves recognizing various activities or movement patterns, such as walking, running, stair ascent, stair descent, and sitting [3]. The goal is to accurately and rapidly detect the intended locomotion modes of assistive device users by analyzing real-time input signals, including kinematic, dynamic, and neuromuscular data. Commonly estimated locomotion modes include level ground walking, sit-to-stand transitions, stair ascent, and descent, and ramp ascent and descent [3]–[5].

Wearable sensors such as inertial measurement units (IMUs), force sensors, and electromyographic sensors, are

widely used for locomotion mode detection [4]. These studies often use feature extraction techniques to identify the unique characteristics of different activities, followed by classification algorithms to detect the activities based on the extracted features [6]–[8]. The complexity of these different classification algorithms varies from simple threshold-based methods to more advanced algorithms such as deep learning approaches [5], [9], [10].

Reported accuracies vary across different studies and depend on factors such as choice of sensors, feature extraction methods, and classification algorithms [11], [12]. Most of the time the performance of the selected techniques is analyzed based on accuracy, sensitivity, and specificity. However, for onboard real-time implementation of suggested strategies, the low computational cost is also important [13], [14]. Since the performance of an assistive device is strongly affected by the response time or delay, an accurate but also fast transition detection strategy is essential [7], [15], [16].

B. Transition Detection

While the existing classification methods excel in locomotion type identification, many of these methods focus on steady-state activity detection for several locomotion modes [4], [17]. However, detecting the transitions between different activities is crucial from the perspective of control of a lower-limb exoskeleton to be able to assist promptly with changes in locomotion, ensuring smooth human-robot interaction and enhancing the safety and efficiency of lower-limb exoskeletons [1], [8], [18]–[21]. This necessitates the development of specialized algorithms that focus on transition detection rather than continuous activity recognition.

Most studies rely heavily on sensors placed on the human body and often lack real-time experimental results integrated into lower-limb assistive devices [14], [20], [22]–[25]. Few studies have conducted experiments with exoskeletons, with many focusing on offline recognition and analysis, and even fewer exploring online recognition in real-time conditions [26].

In the field of lower-limb prosthesis, multiple methodologies are developed to achieve high real-time performance in recognizing different locomotion types for intuitive prosthetic control [19], [27], [28]. However, the identification of transitions between locomotion modes with lower-limb exoskeletons has not been studied as comprehensively as in prosthetic systems. A review article [26] highlights that only three studies investigated the transitions between locomotion modes among the eight studies focused on orthoses or exoskeletons. A more recent review [29], indicates an increasing number of studies aimed at detecting transitions between locomotion modes.

Long et al. [30] optimized support vector machine (SVM) with particle swarm techniques for a knee exoskeleton to identify five modes: level walking, stair and ramp ascent/descent, and transitions using ground reaction forces and orientation data. Tested with three subjects, the approach achieved low error rates but depended on future steps, limiting real-time applicability. Wang et al. [31] used a Long Short-Term Memory (LSTM) network on a soft knee exoskeleton to

detect level walking, stair ascent/descent, and transitions with 98.2% steady-state accuracy, though with a recognition delay of nearly one step. Zhou et al. [22] employed SVM with IMU data for similar modes on a unilateral knee exoskeleton, while Zhang et al. [8] used random forests on a soft hip exosuit to detect level walking and stair ascent/descent with over 90% accuracy. However, these approaches rely on fixed-length sliding windows, potentially limiting adaptability to variable walking speeds.

Liu and Wang, [32] implemented SVM to recognize the locomotion mode for a unilateral knee exoskeleton together with recognition of sitting. Their experimental results demonstrated that the real-time recognition with two IMUs obtained satisfactory recognition accuracy and low delay time. A fuzzy logic-based algorithm for locomotion and transition mode recognition using inertial sensors mounted on a hip joint exoskeleton is proposed by Du et al. [33]. This approach overcomes subject-dependent parameters in data training, avoiding a training procedure per subject. In contrast, subject-independent locomotion mode classification for a hip exoskeleton is suggested by [34] based on a deep convolutional neural network. Although this suggested strategy seems to be promising without fine-tuning subject-specific parameters, it has only been validated in offline scenarios.

Most of the traditional machine learning (ML) approaches are efficient at handling complex patterns, generalizing them effectively, and offering versatility through various algorithms. However, they often require extensive feature engineering and are sensitive to feature quality [35], which can limit scalability. In contrast, deep learning methods can automatically learn features from raw data, excel at capturing complex patterns, and scale well with the availability of large datasets. Despite these benefits, deep learning models demand significant amounts of labeled data, are computationally intensive, and often lack interpretability [35]. Given the constraints of data availability and limited computational resources in assistive devices, this study utilizes an ML-trained threshold-based (TH) method. Unlike manual threshold setting, we employ traditional machine learning approaches to enhance the generalizability of our method, as suggested by Cheng et al. [1].

C. Importance of Personalization

In our previous study [2], the ML-trained TH-method effectively captured the dynamics of transitions based on human subject experiments. However, it did not detect all transitions in every scenario, as subjects exhibited varying dynamics. While the method for detecting transitions between locomotion modes was generally effective across a diverse user base, we identified the need for subject and/or system-specific optimization to accommodate individual differences, especially when exoskeletons impose greater kinematic constraints on user movements.

It has been demonstrated that inter-subject variability in response to any given assistive strategy suggests that device parameters beneficial to one subject may hinder another [36]. This leads to the hypothesis that overall performance across subjects could be improved by tuning control parameters for

each individual [37], [38]. The dual objectives of personalization and generalization present a fundamental challenge in the development of adaptive control systems for assistive devices.

In the literature on lower-limb exoskeletons, initial approaches to personalization have relied on subject-specific training data [37]. However, effective personalization is often constrained by the impracticality of lengthy evaluation periods [39]–[41]. To overcome this challenge, Bayesian optimization, an efficient global optimization strategy, is adopted for its data efficiency and noise tolerance [38], [42], [43]. Bayesian optimization is utilized in a human-in-the-loop (HIL) strategy to reduce the users walking energy consumption using a wearable robot [37], [40]. The HIL Bayesian optimization has been developed to minimize overall experiment time [44]. This minimal experimental time is crucial when prolonged physical exertion is challenging, especially for individuals with impaired mobility.

Building on prior research, our work leverages data from real-time experiments to improve transition detection accuracy by addressing system- and user-specific variability through a statistical-based approach and Bayesian optimization. Our findings show that personalized adjustments can remarkably improve the adaptability and effectiveness of lower-limb exoskeletons, paving the way for more responsive and user-centered assistive technologies.

D. Contributions

The major contributions of this study are the following:

- This study rigorously evaluates the ML-trained threshold-based algorithm with two distinct lower-limb exoskeletons, eWalk and autonomyo. The results demonstrate the algorithm’s versatility and its ability to adapt to different lower-limb exoskeletons with varied design constraints, validating its broader applicability.
- We introduce a statistics-based approach and Bayesian optimization to personalize FSM thresholds. We show through experimental validation that these techniques tailored the detection algorithms to individual gait patterns and system-specific characteristics, enhancing the reliability of transition detection. Additionally, we developed a method to address human-exoskeleton joint alignment issues.
- We provide an open-source dataset of lower-limb kinematics from experiments with eWalk and autonomyo, encompassing data from 18 subjects in total with two exoskeletons across four locomotion modes (walking, sitting, stair ascent, and stair descent) and the transitions between them. This dataset is a valuable resource for advancing research and development in locomotion mode detection and control strategies for lower-limb exoskeletons, and it facilitates comparative studies.

III. METHODS

A. Training Dataset

To develop the locomotion transition recognition algorithm, human gait kinematics and kinetics are studied across various

scenarios using several public datasets [45]–[51], and the public dataset [52] is used to train classifiers offline, with gait data from ten healthy subjects captured using a 10-camera Vicon T40 system. The training dataset is constructed as described in [1]. This dataset involves several activities including walking, stair ascending/descending, sitting, and standing with continuous variations and transitions between activities. Transitions between different locomotion modes are noted as Walk to Sit ($W \rightarrow S$), Sit to Walk ($S \rightarrow W$), Walk to Stair Ascend ($W \rightarrow SA$), Stair Ascend to Walk ($SA \rightarrow W$), Walk to Stair Descend ($W \rightarrow SD$), Stair Descend to Walk ($SD \rightarrow W$) and finally all the steady state cases are notated with *mode*. The dataset was split into 90% for training and validation, with 72% for offline training and 18% for FSM validation, and the remaining 10% for testing.

B. Features and State-Machine

Based on [1], kinematics-based classification features called instantaneous characteristic features (ICFs) are derived from thigh angle (θ_{th}) and thigh velocity ($\dot{\theta}_{th}$). Three ICFs (ICF-1, ICF-2, ICF-3) are used to classify transitions between Walk and Sit, Walk and Stair Ascent, and Walk and Stair Descent at three specific moments: (1) maximum hip flexion (MHF), (2) heel strike (HS), and (3) thigh angle in a specified range (THR) defined as $\theta_{th} \in [62, 75]_{ewalk}$ and $[55, 70]_{autonomy}$. MHF and HS are used for general locomotion transitions, while THR is specific to Walk and Sit transitions. ICF-1 is θ_{th} at MHF $\theta_{th, MHF}$, ICF-2 is the difference $\theta_{th, MHF} - \theta_{th, HS}$ and ICF-3 is $\dot{\theta}_{th}$, when $\theta_{th} \in THR$ as shown in Table I.

We use the FSM [1] with four states Sit, Walk, Stair Ascent, and Stair Descent to address six transition detection scenarios, as shown in Fig. 2. The FSM combines level walking, standing, and ramp walking into a unified state. Transition detection relies on ICF detectors to identify key moments, such as MHF and HS, based on thigh angle and ground reaction force data.

C. Classification Algorithms

Before testing in real-world scenarios, various machine learning algorithms (e.g., Linear support vector machines (SVM), Logistic Regression (LR), k-Nearest Neighbors, Nave

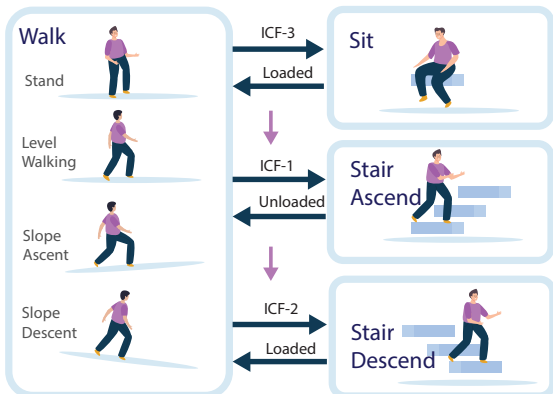


Fig. 2: The finite state machine suggested by Cheng et al. with the updated value of thigh boundary for ICF-3 [1].

TABLE I: The derived features Instantaneous characteristic features (ICFs) used to detect transitions between distinct locomotion modes as suggested by Cheng et al. [1]. The table provides thresholds (Thr.) for each feature on the thigh angle trajectory (θ_{th}) in *deg* and thigh angular velocity ($\dot{\theta}_{th}$) in *deg/s* for the eWalk and autonomy (auto.) exoskeletons. MHF refers to maximum hip flexion, and HS represents heel strike.

Transition	Class. feat.	Definition	Thr. eWalk	Thr. auto.
$W \rightarrow S$	ICF-3	$\dot{\theta}_{th}$, when $\theta_{th} \in THR$	23.32	23.32
$S \rightarrow W$	ICF-3	$\dot{\theta}_{th}$, when $\theta_{th} \in THR$	-4.32	-4.32
$W \rightarrow SA$	ICF-1	θ_{th} at MHF $\theta_{th, MHF}$	50.52	50.52
$SA \rightarrow W$	ICF-1	θ_{th} at MHF $\theta_{th, MHF}$	51.21	51.21
$W \rightarrow SD$	ICF-2	The difference $\theta_{th, MHF} - \theta_{th, HS}$	10.37	13.37
$SD \rightarrow W$	ICF-2	The difference $\theta_{th, MHF} - \theta_{th, HS}$	9.62	9.62

TABLE II: Training and test accuracies with selected algorithms for each classifier. LR refers to logistic regression and SVM to support vector machine.

Transition	Algorithm	Training Acc.	Test Acc.
$W \rightarrow S$	Linear SVM	86.94%	90.91%
$S \rightarrow W$	LR	95.07%	100.0%
$W \rightarrow SA$	LR	91.44%	89.36%
$SA \rightarrow W$	LR	81.67%	86.89%
$W \rightarrow SD$	LR	93.20%	94.38%
$SD \rightarrow W$	LR	97.25%	96.55%

Bayes (NB), Random Forest (RF), Gradient Boosting (GB)) were used to train classifiers offline using the Scikit-learn (v1.3.0) library in Python (v3.11.4) [53]. Hyperparameters were heuristically tuned based on accuracy, and the best-performing algorithm in terms of test accuracy was selected. We use a Gaussian kernel for NB, we set $k = 5$, and use Euclidean distance with equal distance weight for KNN. In the RF algorithm, we set 12 minimum splits and 30 number of estimators; in GB, instead, 2 and 100 respectively, with learning rate $\alpha = 0.1$. Default parameters of the scikit-learn library were used for LR and Linear SVM. After comparative analysis, Linear SVM and LR were found to be the best-performing algorithms. Training and test accuracy for the best-performing algorithms for each transition are reported in Table II.

D. ML-Trained Threshold-Based Method Implementation

Many assistive devices are resource-constrained embedded systems that require computational efficiency for real-time operations to enable quick and responsive control actions. Our previous work introduced an ML-trained TH-based implementation to enhance this efficiency, demonstrating improved computational performance, ease of implementation, and interpretability of the new method [2]. The approach from [1], involves training ML classifiers based on a 1-D feature space, which establishes thresholds on significant classification features (ICFs) for various transitions. However, deploying ML models on embedded systems can increase computational costs and introduce delays. By deriving thresholds from offline training, these models can be replaced with simple *if/else* conditions, ensuring efficient, real-time performance. Thus the classifiers are implemented using thresholds in this study as well.

E. Hardware

In this study, we used two distinct lower-limb exoskeletons, eWalk and autonomyo, both developed at EPFL REHAssist research group. The exoskeleton eWalk (eWalk v2) is designed to provide partial assistance for hip flexion/extension (flex./ext.) movement in collaboration with the company Sonceboz [54], [55]. eWalk has 2 active degrees of freedom which are actuated with DC servo motors as shown in Fig. 3. eWalk allows abduction/adduction (abd./add.) and the internal rotation of the hip to minimize the kinematic constraints imposed by the exoskeleton on natural walking.

The lower-limb exoskeleton autonomyo is developed in collaboration with Faulhaber Drive Systems SA to partially assist people with walking impairments due to neuromuscular deficit [56], [57]. The autonomyo exoskeleton (autonomyo v2) has 3 active and 3 passive degrees of freedom per leg. The 3 actives are on the hip (abd./add. and flex./ext.) and knee (flex./ext.) joints as shown in Fig. 3. The remaining passives are at the ankle joint (eversion/inversion, dorsiflexion/plantar flexion, and abd./add.). For hip and knee flexion/extension actuation, each unit consists of a brushless motor and a corresponding gearbox with a 108:1 transmission ratio. An additional cable transmission (2.6:1) is utilized for hip and knee flex./ext. actuation, while a ball screw transmission is used for hip abd./add.. There are integrated torque sensors on the actuator side for the hip and knee flex./ext..

Joints are measured on the motor side for both devices. The zero position of the joints is initialized by the homing technique, and with the absolute encoders on the joints for eWalk and autonomyo, respectively. The torso angle with respect to the gravity vector is measured with an IMU (6-axis MPU6050) located on the back module of autonomyo. Ground reaction forces (GRFs) are measured by instrumented



Fig. 3: The lower-limb exoskeleton autonomyo on the left side and the hip orthosis eWalk on the right side.

soles in both of the devices where on eWalk force sensitive resistor (FSR) based insole is used and eight load cells per foot is utilized for autonomyo.

Both exoskeletons are equipped with an embedded computer (BeagleBone Black, Texas Instruments, USA) that collects and keeps the log of all the sensory data on the embedded computer. Wireless communication with both devices is established through a Wi-Fi module.

F. Human-Exoskeleton Joint Misalignment

In real-world exoskeleton applications, discrepancies in joint angle measurements often arise due to kinematic constraints and misalignments, such as rotational offsets and center of rotation shifts, with restrictive systems like autonomyo showing greater deviations than more flexible designs like eWalk.

Previous work addressed these issues through ergonomic and self-aligning mechanisms [58]–[61]. Instead of focusing on hardware improvements, we propose a versatile mapping algorithm inspired by machine learning regression techniques [62] to correct misalignments and improve data accuracy across different exoskeleton systems. Our focus is on the hip flex./ext. joint in autonomyo, where a simple mapping function:

$$f(\mathbf{w}, \phi(x)) = \phi(x)\mathbf{w} \rightarrow t \quad (1)$$

aligns measured joint angles with literature data [52]. Here, \mathbf{w} represents the weights, ϕ is a vector of functions of the input x , and t is the corrected angle. We aim at setting the free parameters \mathbf{w} such that the difference between the function's output f and the desired output t is minimized. To achieve this, we define an optimization problem using a sum of squares loss function L measuring the squared difference between f and t pairs in the dataset:

$$\begin{aligned} L(\mathbf{w}) &= (\mathbf{t} - f(\mathbf{w}, \phi(x)))^T (\mathbf{t} - f(\mathbf{w}, \phi(x))) \\ &= (\mathbf{t} - \phi(x)\mathbf{w})^T (\mathbf{t} - \phi(x)\mathbf{w}) \end{aligned} \quad (2)$$

And we minimize it with respect to the free parameters \mathbf{w} :

$$\nabla_{\mathbf{w}} L(\mathbf{w}) = 0 \longrightarrow \mathbf{w}_{opt} = [\phi(x)^T \phi(x)]^{-1} \phi(x)^T \mathbf{t} \quad (3)$$

The final function takes into account position, velocity, and acceleration:

$$f(x, \dot{x}, \ddot{x}) \rightarrow t, \quad f: \mathbb{R}^3 \rightarrow \mathbb{R} \quad (4)$$

where $\mathbf{w} = [w_0, w_1, w_2, w_3, w_4, w_5, w_6]^T$ are the trainable parameters coupled with the linear and nonlinear combinations of position, velocity, and acceleration. Specifically:

$$\phi(x) = [1, x, \dot{x}, \ddot{x}, x \cdot \dot{x}, x \cdot \ddot{x}, \dot{x} \cdot \ddot{x}] \quad (5)$$

At each time step, we combine the encoder's measured hip position (x), velocity (\dot{x}), and acceleration (\ddot{x}) to produce a corrected hip angle (t). As we only have 7 trainable parameters (\mathbf{w}) to avoid underfitting we train the model on 12 walk-to-stair ascend (W→SA) transition cycles from 10 subjects, considered as the most representative of the process, and using literature means as ground truth (GT).

We evaluate the training performance by assessing generalizability across subjects, visually confirming the mapping, and calculating the root mean squared error (RMSE) on the training dataset. The effectiveness of this formulation comes from the flexibility of the functions ϕ , which can be chosen as arbitrary nonlinear functions of the input x and its derivatives to handle data nonlinearity. The weights w_i are optimized to fit specific datasets or processes. In the end, this method offers a flexible, system-agnostic solution for improving exoskeleton data accuracy.

G. User Specific or System Specific Optimization Methods

The trade-off between computational efficiency and generalization capability led to the use of the proposed FSM for transition detection. However, due to this trade-off, the transition detection accuracy may decrease when the FSM encounters gait data from subjects who differ considerably from the training set, especially when using various locomotion support systems tailored for different populations. To address these challenges, the following sections introduce fine-tuning techniques aimed at enhancing detection accuracy, particularly for subjects who represent outlier cases.

1) Statistics-Based Tuning

We developed the *Statistics-Based tuning* (SBA) approach to adapt thresholds by analyzing statistical differences between training and subject-specific data. The Finite-State Machine uses thresholds as upper and lower bounds to detect transitions. For example, as shown in Fig. 4, the ICF associated during SA→W and W→SA transitions must exceed or fall below trained thresholds (th_{W-SA} and th_{SA-W}) for detection, in this sense, they are defined as lower and upper bounded respectively. This approach applies to all transition pairs.

Fig. 4-B illustrates a scenario where the threshold, tuned on the training population, is too high to detect transitions in the new population, causing the FSM with initially trained thresholds underperform. To improve transition detection performance, we propose lowering the thresholds based on the new population's statistical properties, as indicated by the arrow in the figure. This adjustment scales the training thresholds to better fit the new data, as defined by the following formula:

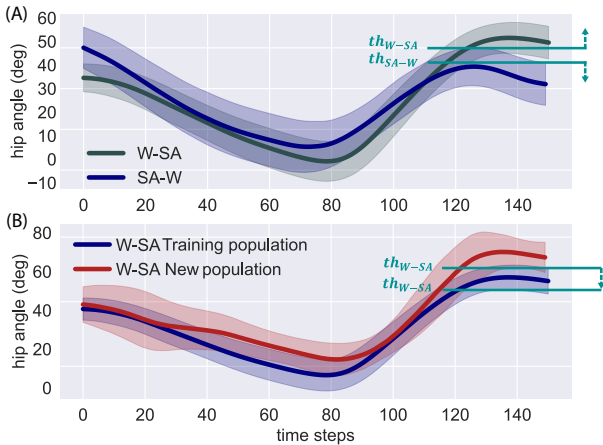


Fig. 4: Visualisation of the upper and lower bounded transitions.

$$TH_{new} = TH_{tr} \cdot \frac{\text{mean}(ICF_i^{new}) \pm \text{std}(ICF_i^{new})}{\text{mean}(ICF_i^{tr}) \pm \text{std}(ICF_i^{tr})} \quad (6)$$

Where TH_{tr} represents the old threshold from offline training, and TH_{new} is the adjusted threshold after statistics-based tuning. A $+$ sign is used for lower bound transition cases, while a $-$ sign is used otherwise. $ICF_i^{new/tr}$ denotes the feature for the specific transition cycle in the new or training data. Summing up, we extract ICF_i for both populations and use Eq. 6 to adjust the threshold.

2) Bayesian Optimization-based Tuning

Although SBA allows us to tune the FSM thresholds for individuals, formally the thresholds can be optimized by solving an optimization problem as:

$$\begin{aligned} \mathbf{TH}^* &= \underset{\mathbf{TH} \in \mathbb{R}^n}{\text{argmin}} J(\mathbf{TH}) \\ &\text{subject to } \mathbf{TH} \in \Omega \end{aligned} \quad (7)$$

Here, J is an objective function to be minimized to maximize the output accuracy, and \mathbf{TH} denotes the optimization thresholds. We use *Bayesian Optimization* (BO) to fine-tune these thresholds for specific data when the impact of threshold changes on final performances is unclear and the explicit form of $J(\mathbf{TH})$ is unavailable [63]. BO iteratively samples the parameter-output relationship and uses an *acquisition function* to guide optimization with minimal experiments.

To estimate the objective function, we use Gaussian Processes with a Radial Basis Function kernel, implemented via the GPy library in Python [64]. This RBF kernel is selected for its smoothness, higher-order derivatives, as well as the capability to provide both mean and uncertainty values as a consequence of data fitting [65]. The GP fitting produces a *surrogate function* $S(\mathbf{TH})$ in terms of mean and variance, which we use to formulate the acquisition function as follows:

$$A(\mathbf{TH}) = k * \text{mean}(S(\mathbf{TH})) \pm (1-k) * \text{std}(S(\mathbf{TH})) \quad (8)$$

The parameter k in BO balances exploration and exploitation. Since our search space includes multiple local minima, we set $k = 0.5$ to prioritize balanced exploration and rapid convergence to the global minimum. The acquisition function A , derived from a surrogate function, estimates the objective function and reflects the relationship between parameters and performance. Therefore, BO iteratively solves two optimization problems simultaneously: it refines this differentiable surrogate function with new and past data and minimizes the acquisition function to find optimal thresholds. As a result, instead of solving Eq. 7, the process recursively solves the following:

$$\begin{aligned} \mathbf{TH}^* &= \underset{\mathbf{TH} \in \mathbb{R}^n}{\text{argmin}} A(\mathbf{TH}) \\ &\text{subject to } \mathbf{TH} \in \Omega \end{aligned} \quad (9)$$

Algorithm 1 provides a pseudocode of the BO process. We optimize thresholds in pairs, and the searching space Ω per each one is set $TH_{W-S/S-W} \in [-60, 60]$, $TH_{W-SA/SA-W} \in [30, 65]$, $TH_{W-SD/SD-W} \in [0, 25]$.

The objective function $J(TH_{transit1}, TH_{transit2}) = J(\mathbf{TH})$, is evaluated using the following pseudocode given in Algorithm 2.

Algorithm 1 Bayesian Optimization Process

```

1: Variables:  $J, \mathbf{TH}$ 
2: while not convergence condition do
3:    $J, \mathbf{TH} \leftarrow \text{new\_sample}$   $\triangleright$  from experiment/simulation
4:   estimate  $J(\mathbf{TH})$   $\triangleright$  By fitting  $\{J, \mathbf{TH}\}$  pairs with GP
5:   formulate  $A(\mathbf{TH})$ 
6:   suggest  $\mathbf{TH}_{\text{next}}$  from  $\mathbf{TH}_{\text{next}} = \text{argmin}_{\mathbf{TH}} A(\mathbf{TH})$ 
7: end while

```

Algorithm 2 Objective function evaluation

```

1: if  $GT = \text{class1}$  and  $\text{FSM\_output} \neq \text{class1}$  then
2:    $J_{j+1}(\mathbf{TH}) \leftarrow J_j(\mathbf{TH}) + C_1$ 
3: end if
4: if  $\text{transition\_to\_class1\_happened\_before}$  then
5:   if  $GT = \text{class}$  and  $\text{Output\_FSM} \neq \text{class}$  then
6:      $J_{j+1}(\mathbf{TH}) \leftarrow J_j(\mathbf{TH}) + C_2$ 
7:   end if
8: end if

```

In this context, *class1* refers to the classes the algorithm can detect from “Walking” (e.g., Sit, Stair Ascend, Stair Descend), while *class* always represents Walk. *GT* requires supervised experiments with labeled data for BO. The penalty constants C_1 and C_2 are heuristically set to 0.005 and 0.001, respectively, with C_1 being higher to reduce the risk of getting stuck in a local minimum where the system prioritizes the recognition of the second transition. By assigning a higher penalty to the first transition in a sequence, we ensure it is recognized first. Thus, the FSM is penalized whenever it outputs a class different from the ground truth, with greater penalties the longer the time the FSM takes to detect the transition. Furthermore, additional penalties are applied during $W \rightarrow SA/SA \rightarrow W$ and $W \rightarrow SD/SD \rightarrow W$ optimizations if threshold values are excessively high or low as described in Algorithm 3 and Algorithm 4.

Algorithm 3 Regularization $W \rightarrow SA/SA \rightarrow W$ optimization

```

1: if any  $\mathbf{TH}_{\text{current}} > 55^\circ$  then
2:    $J_j = J_j + \frac{\alpha}{2} \|\mathbf{TH} - [55, 55]\|_2^2$ 
3: end if

```

Algorithm 4 Regularization $W \rightarrow SD/SD \rightarrow W$ optimization

```

1: if any  $\mathbf{TH}_{\text{current}} < 5^\circ$  then
2:    $J_j = J_j + \frac{\alpha}{2} \|\mathbf{TH} - [5, 5]\|_2^2$ 
3: end if

```

Where, $\mathbf{TH} = [TH_{\text{transit1}}, TH_{\text{transit2}}]$, and α is a parameter governing the strength of the regularization, with no regularization when $\alpha = 0$ [66]. In our case, we heuristically set $\alpha = 2 * 10^{-5}$. This regularization term, inspired by neural network weight decay strategies [67], helps prevent getting stuck in local minima while expanding the search space for optimal solutions. For instance, in $W \rightarrow SA/SA \rightarrow W$ optimization, setting a too high threshold for $W \rightarrow SA$ transition detection causes the algorithm to always classify as

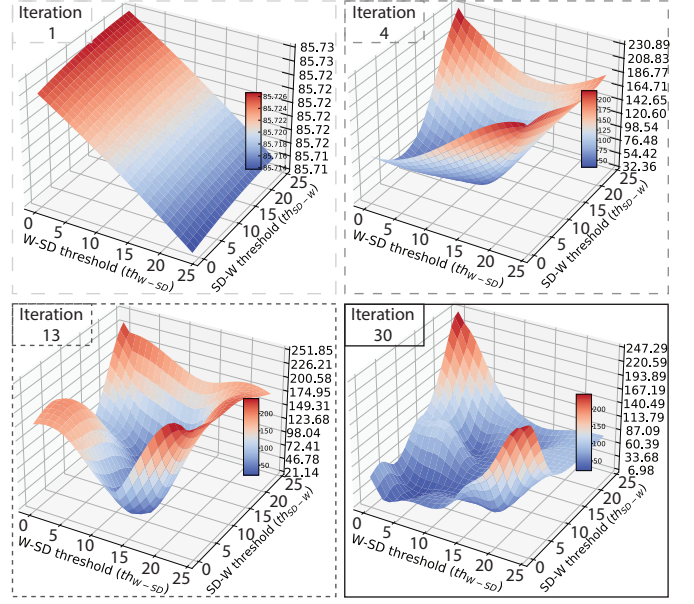


Fig. 5: Bayesian Optimization process for subject 5 wearing eWalk for one of the test scenarios.

“Walking” and missing the “Stair Ascending” transition thus prioritizing one transition over the other and creating a local minimum. By optimizing both transitions simultaneously and introducing this regularization term, we reduce the risk of encountering such local minimum.

As detailed in Section IV, our experimental scenario included 5 transitions per type per subject. We applied BO to subjects and transitions with poor performance, using 2 transitions for training and the remaining 3 for accuracy evaluation with the optimized thresholds. To determine the appropriate number of iterations for BO to effectively explore the search space and provide an accurate estimate of the objective function, we conducted a Grid Search in parallel with the optimization process. Based on the results, we set the number of BO iterations to 30.

Evolution of the acquisition function in BO

The iterative updates of the acquisition function throughout the BO process are illustrated in Fig. 5. At Iteration 1, the acquisition function begins with a flat initial guess, indicating a lack of information about the objective function’s landscape. As the optimization progresses to Iteration 4, the acquisition function starts to explore the search space, revealing the initial contours of potential areas for optimization. By Iteration 13, the function displays more distinct peaks and valleys, reflecting a refined understanding of the objective landscape and identifying promising regions for further exploration. Finally, at Iteration 30, the acquisition function has notably evolved, showing well-defined global and local minima that correspond to optimal thresholds. This progression demonstrates the BO process’s balance between exploration and exploitation, as it efficiently searches the parameter space to find the best solutions while continuously refining its model of the objective function.

3) Discrete Grid Search Based Tuning

The discrete Grid Search algorithm (GSA) is implemented as a baseline method to optimize the thresholds since it is one

of the most common tuning approaches given its simplicity and straightforward implementation. The Grid Search (or parameter sweeping) evaluates a fixed number of conditions and then selects the condition with the lowest average cost.

The design space Ω is defined as follows: $TH_{W-S/S-W} \in [-60, 60]$, $TH_{W-SA/SA-W} \in [30, 65]$, $TH_{W-SD/SD-W} \in [0, 25]$. For $W \rightarrow SA/SA \rightarrow W$ and $W \rightarrow SD/SD \rightarrow W$ transitions, the space is discretized in 2.5 degree increments, while for $W \rightarrow S/S \rightarrow W$ it is discretized in 10-degree increments. The same cost function, as introduced in the previous section, is evaluated at each discretization point. The resulting optimization serves as a ground truth comparison for BO.

IV. REAL-TIME

EXPERIMENTS WITH eWALK AND AUTONOMYO

The experiment tested four locomotion modes: level walking, stair ascent, stair descent, and sitting along with six transitions between these modes ($W \rightarrow SA$, $SA \rightarrow W$, $W \rightarrow S$, $S \rightarrow W$, $W \rightarrow SD$, and $SD \rightarrow W$) in the environment shown in Fig 1. Subjects completed 15-step stairs and selected their walking speed and sitting position. Each transition was repeated 50 times per exoskeleton, with each subject performing five trials.

For the experiments, eligible adults are aged 18-65, height of 160-200 cm, have EU shoe size 38-45, can consent and follow the study, and are in good health for walking without problems. Those with systemic disorders, seeking treatment, psychiatric/cognitive impairments, insufficient language skills, under guardianship, and pregnant/nursing are excluded. During the tests, ten healthy subjects with the age of 25.6 ± 2.76 years, a height of 178.4 ± 8.1 cm, and a body mass of 71.9 ± 9.68 kg were asked to perform the trial with eWalk. For the tests with autonomy ten healthy subjects with the age of 26.9 ± 3.42 years, the height of 178.2 ± 8.65 cm, and a body mass of 72.2 ± 13.44 kg were asked to participate. During this test, participants were constantly monitored and helped if needed, to avoid any risk of accident. All participants provided written and informed consent, according to the ethical conduct defined by the EPFL Human Research Ethics Committee, which follows the standards set by the declaration of Helsinki and the Oviedo Convention.

During the experiments, eWalk is utilized in passive mode due to the transparent nature of the device with low mass and low friction, and passive back-drivability where autonomy is utilized in the zero-torque mode which enables transparency without adding additional assistance.

The ground truth data are labeled during the experimental procedure. An observer assigned the ground truth label for each transition and steady-state locomotion type. This label is logged in real-time together with the rest of the data from the exoskeletons.

V. RESULTS

A. Joint Trajectories

In this study, we aimed to capture natural human movement by utilizing joint angle measurements. Fig. 6 presents the hip and thigh angle trajectories from experiments with both the eWalk and autonomy exoskeletons, respectively. The

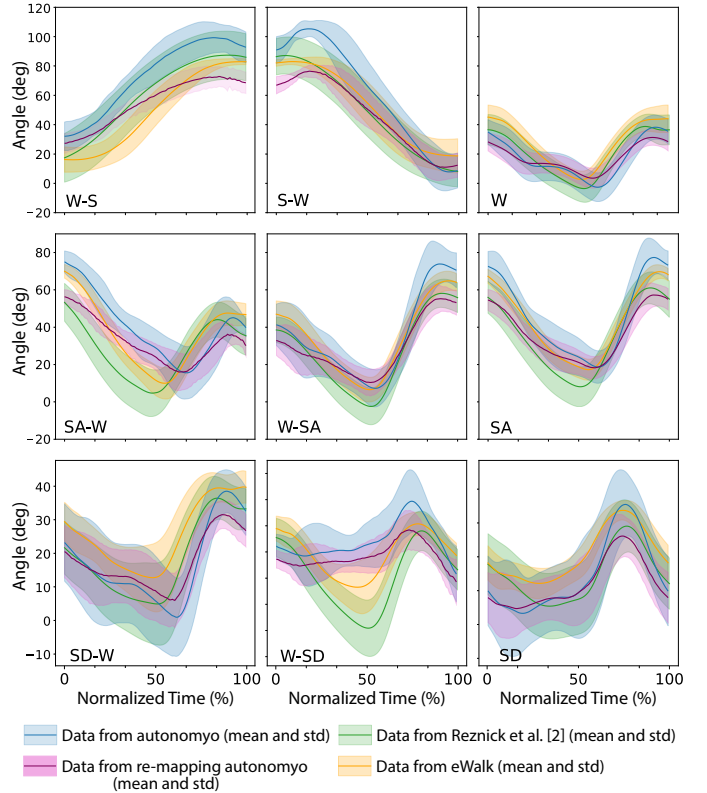


Fig. 6: Hip and thigh angle trajectories from measurements of eWalk and autonomy experiments, respectively, for tested locomotion modes together with the re-mapped autonomy joint angles by using the mapping function for tested locomotion modes in comparison with literature data given in [52].

trajectories for $W \rightarrow S$, $S \rightarrow W$, $W \rightarrow SA$, $SA \rightarrow W$, $W \rightarrow SD$, $SD \rightarrow W$, W , SA and SD are shown in comparison with literature data from [52]. These comparisons highlight the natural movement patterns observed during the tests and how closely they align with established biomechanical data.

The labeled time-series data from the experiments are shared as accompanying data in [68]. An example script for exploring the dataset is also available in the repository.

B. Effect of Joint Misalignment

Despite the alignment seen in some cases, the data from autonomy experiments displayed discrepancies due to joint misalignment issues between the exoskeleton and the human hip joint. To address this, we train the mapping function on the dataset $D = \{\mathbf{x}, \mathbf{t}\}$, where \mathbf{t} consists of $W \rightarrow SA$ transition cycles from the literature and \mathbf{x} comes from autonomy. The resulting optimal weights are presented in Table III. We avoid normalization to minimize unnecessary and keep the model as light as possible, resulting in the different scales of the weights.

TABLE III: Mapping function's weights outcome from the training

w_0	w_1	w_2	w_3	w_4	w_5	w_6
5.7	6.7e-1	3.3e-2	3.1e-4	-4.6e-4	5.7e-6	-2.5e-6

Fig. 7 shows that applying the mapping function reduces the mean MHF value from 73.87° to 55.27° , aligning it

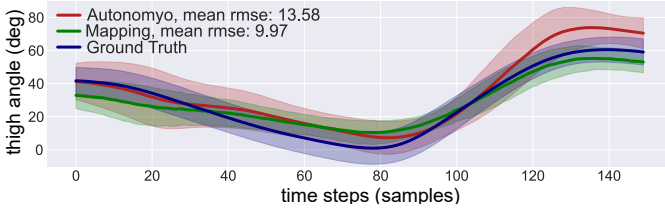


Fig. 7: Mapping outcome on the training dataset that shows the ground truth, measurement of hip flex/ext angle and re-mapped joint angles.

more closely with the literature value of 60.55° [52]. The mean standard deviation across gait cycles decreases from 17.48° to 11.95° with standard deviation presented in the literature data 10.49° [52]. Additionally, the mean RMSE between the literature data and mapped joint angle compared to unprocessed autonomy gait data is reduced by 3.61° .

Fig. 8 illustrates the regression feature space with one (x) and two (x, \dot{x}) input features, showing the nonlinear relationship between features extracted from autonomy data and the corresponding hip angle according to ground truth data. In both cases, the mapped outputs closely follow the ground truth nonlinearity without overfitting, demonstrating the mapping function’s potential to accurately track joint dynamics.

To validate the generalizability of the mapping function, we applied the mapping process to other locomotion modes and the transitions between them, as presented in Fig. 6. The re-mapped joint angles exhibited a notable reduction in data variance, enhancing our ability to capture natural human movement with greater consistency.

C. Transition Detection Performance

The recognition accuracy is defined as shown in Eq. 10:

$$A = \frac{N_{\text{correctly detected transitions}}}{N_{\text{total transitions}}} \cdot 100 \quad (10)$$

where $N_{\text{correctly detected transitions}}$ is the detected transitions at the correct moment and $N_{\text{total transitions}}$ was the number of total trials. If the method does not recognize the transition at the transition time or with a maximum one-step delay, it is considered not detected, even if the steady state is correctly classified.

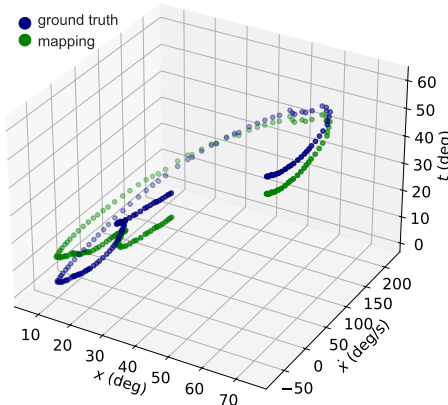


Fig. 8: Comparison of the ground truth data and re-mapped joint angles in 3D.

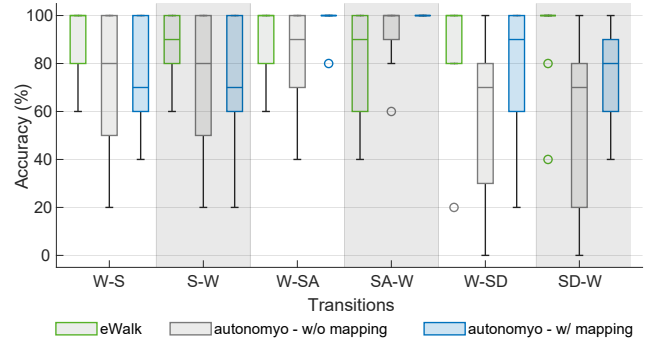


Fig. 9: Real-time recognition accuracy (%) of locomotion transitions from experiments with eWalk and autonomy exoskeletons.

Note that the accuracy reported here is not calculated over all the samples in the collected data but with a binary evaluation based on the detection condition.

The recognition accuracy results are reported in Fig. 9 for the experiments with the eWalk and autonomy exoskeletons. For the autonomy exoskeleton, the results are computed offline after applying the hip flex/ext. mapping function to the experiment log as well. Note that Subjects 3 and 7 were excluded from the autonomy experiment data as they could not comfortably perform the experimental procedure with their natural gait.

The median detection accuracy for the eWalk experiments are reported as 100%, 90%, 100%, 90%, 100% and 100% for the transitions of $W \rightarrow S$, $S \rightarrow W$, $W \rightarrow SA$, $SA \rightarrow W$, $W \rightarrow SD$, and $SD \rightarrow W$, respectively. For the autonomy experiments, the corresponding accuracies were 80%, 80%, 90%, 100%, 70%, and 70%. After utilizing the re-mapped joint angles in the autonomy experiments, the transition detection accuracy changed as follows: $W \rightarrow S$ and $S \rightarrow W$ decreased from 80% to 70%, $W \rightarrow SA$ increased from 90% to 100%, $SA \rightarrow W$ remained at 100%, $W \rightarrow SD$ increased from 70% to 90%, and $SD \rightarrow W$ improved from 70% to 80%. Additionally, the standard deviation was reduced in all transition cases except for $S \rightarrow W$.

D. Transition Detection Performance After Optimization

Fig. 10 shows the transition detection accuracies from eWalk and autonomy experimental data using SBA and BO methods. For eWalk, both SBA and BO effectively improved transition accuracies, with BO providing slightly better results in some transitions. Specifically, for eWalk, tuning the FSM thresholds with SBA increased the mean transition detection accuracy for $W \rightarrow S$ from 92% to 94%, $S \rightarrow W$ from 86% to 90%, $SA \rightarrow W$ from 80% to 88%, $W \rightarrow SD$ from 88% to 92%, and $SD \rightarrow W$ from 92% to 96%. BO achieved the same increases for $W \rightarrow S$, $S \rightarrow W$, and $SA \rightarrow W$ transitions, while further increasing $W \rightarrow SD$ accuracy to 96% and $SD \rightarrow W$ accuracy to 98%. However, for the autonomy, SBA did not yield improvements, while BO enhanced performance across all targeted transitions. BO increased the detection accuracy for $W \rightarrow S$ from 77.5% to 90%, $S \rightarrow W$ from 75% to 90%, $W \rightarrow SD$ from 77.5% to 87.5%, and $SD \rightarrow W$ from 75% to 82.5%.

The final accuracy results for the transition detection for all of the subjects together with the mean accuracy changes after

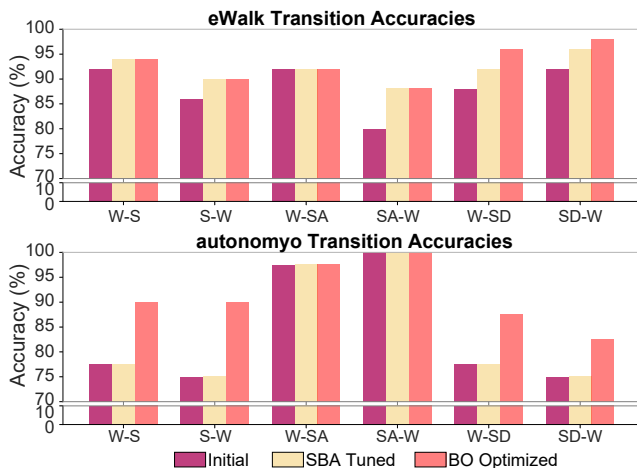


Fig. 10: Changes of the transition detection accuracy results with SBA and BO for eWalk and autonomy.

BO are presented in Fig. 11 and Fig. 12 for the eWalk and autonomy experiments. The Fig. 11 and Fig. 12 illustrate the effectiveness of BO in enhancing transition detection performance at both the group and individual levels.

For the eWalk experiments, most subjects experienced a noticeable improvement in accuracy, indicating that BO effectively fine-tuned the model to account for individual gait patterns and interaction behaviors. For example, for Subject 2, one $W \rightarrow S$ transition was missed before BO, but after optimization, all transitions were correctly detected. Similarly, $S \rightarrow W$ transition detection for Subject 2 improved from 60% to 100%. For Subject 5, $W \rightarrow SD$ transition detection accuracy increased from 20% to 100%, and $SD \rightarrow W$ accuracy rose from 40% to 100%, though no improvement was observed for this subject’s $SA \rightarrow W$ transition accuracy. The mean accuracy changes for eWalk reveal that BO not only increased overall detection rates but also reduced variability among subjects, suggesting a more consistent performance across the diverse user base.

For the autonomy experiments, the results showed varied outcomes across subjects. While some subjects who initially had lower detection accuracies achieved substantial improvements following BO, others exhibited more moderate changes. For example, the $S \rightarrow W$ and $W \rightarrow S$ transition detection accuracy for Subject 6 improved by 40% after BO, reaching 100% accuracy. However, more modest increases were

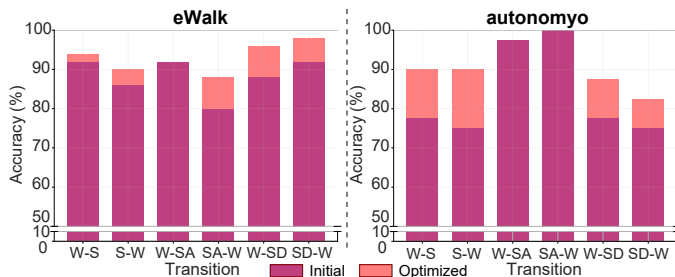


Fig. 11: Changes of the overall mean accuracy results with the subject-specific thresholds after BO for each of the transitions for the eWalk and autonomy experiments.

observed for Subject 5 during $W \rightarrow SD$ and Subject 8 during $SD \rightarrow W$, with only a 20% improvement following threshold personalization. This variability suggests that BO effectively adapted the system to each subjects unique interaction with the exoskeleton, optimizing transition detection based on individual characteristics. Despite the differences in improvement levels, the overall trend indicates that BO enhanced transition detection accuracies across a diverse range of users.

E. Comparison of Bayesian Optimization and Grid Search

Fig. 13 shows the BO process alongside a parallel discrete GSA for optimizing the $W \rightarrow SD/SD \rightarrow W$ transition thresholds for Subject 5 using eWalk. The comparison between the BO acquisition function at the final iteration and the actual objective function derived from GSA reveals a strong similarity, particularly in the location of the global minimum. This indicates that both BO and GSA converge to similar optimal thresholds. However the BO process demonstrates a more efficient optimization, achieving convergence in just 30 iterations, compared to the 100 computations needed for GSA in this case. The final thresholds obtained for each subject across all transitions after BO optimization are summarized in Fig. 14.

F. Computational Time for Optimization

Computation time required to optimize threshold values with BO is investigated in comparison to a discrete GSA for 5 subjects from the experiments with the eWalk exoskeleton. Both BO and GSA were run 10 times per subject on the same machine, equipped with an Apple M1 processor, 8-core CPU, 7-core GPU, and 8GB RAM. Fig. 15 presents the computational time for the optimization with BO and GSA for the five subjects, along with the mean of these five values. On average, GSA took four times longer than BO to optimize the thresholds, highlighting the computational efficiency of BO.

VI. DISCUSSION

The results demonstrate the systems capability to capture natural movement while addressing system- and user-specific variability through personalized threshold tuning via SBA and BO, highlighting its computational efficiency and adaptability. In this section, we rigorously examine the implications of these findings in the context of locomotion mode detection and personalization, while also discussing the limitations and potential directions for future research.

A. Public Dataset of the Joint Trajectories

The joint trajectories captured during the experiments highlight the potential of both the eWalk and autonomy exoskeletons in facilitating natural human movement across various locomotion modes. The consistency between the joint trajectories in our experiments and those reported in the literature [52] reinforces the reliability of the measurements from exoskeletons. This alignment is particularly evident in the eWalk, where the hip flex./ext. angles closely match natural human movement patterns without the exoskeleton. Such accuracy is crucial for ensuring smooth and intuitive

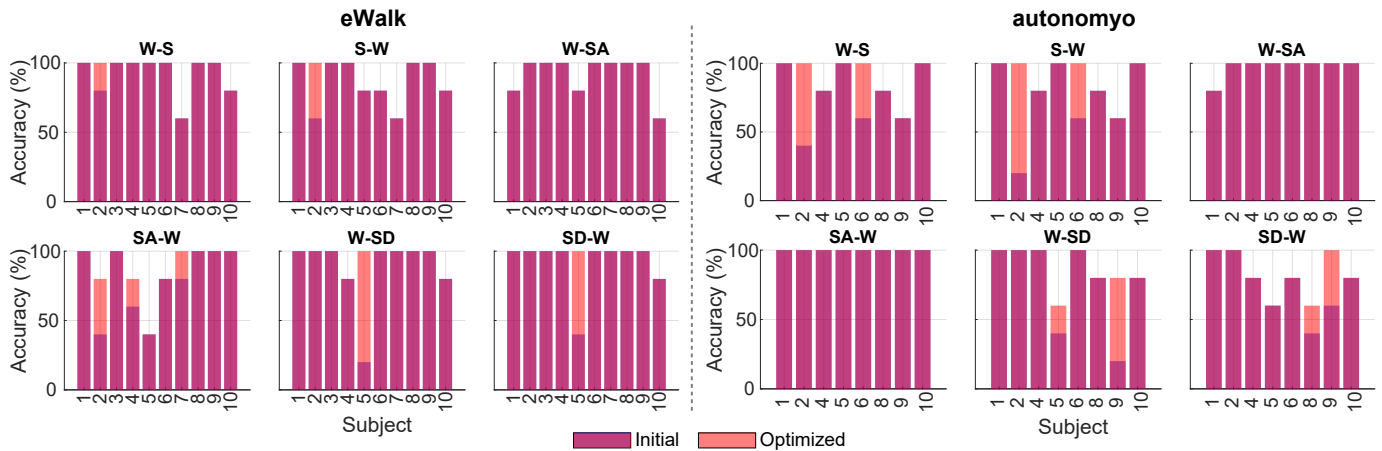


Fig. 12: Changes of the accuracy results of each subjects with the subject-specific thresholds after BO for each of the transitions for the eWalk and autonomy experiments.

human-robot interaction, which directly impacts user comfort and overall system effectiveness in real-world applications.

Despite the growing research on lower-limb exoskeletons, publicly available datasets in this field remain scarce. Most existing datasets focus on non-exoskeleton-assisted gait [47], [52], [69]–[71], limiting opportunities for comparative studies and the development of standardized benchmarks for exoskeletons. This dataset makes a significant contribution by offering joint trajectory data from two exoskeletons, eWalk and autonomy. It provides researchers with a valuable resource to systematically evaluate and compare control strategies, advancing the fields of locomotion mode detection and personalization in assistive robotics.

B. The Importance of the Joint Alignment

Accurate joint trajectory data is essential for improving locomotion mode detection, but joint misalignment between human and exoskeleton joints remains a persistent challenge

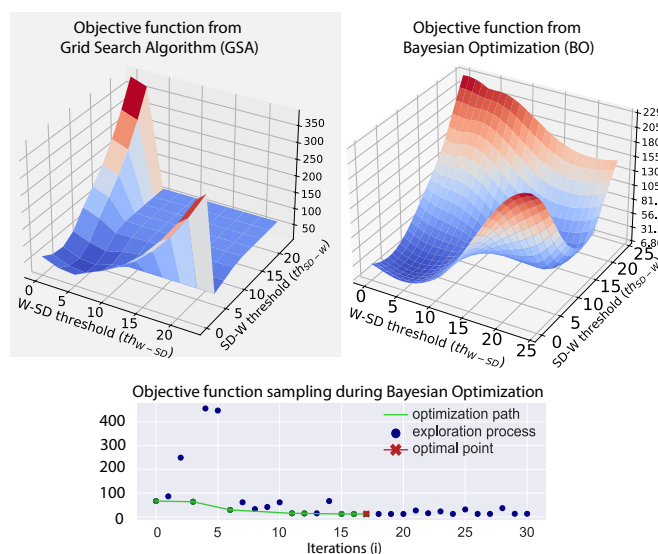


Fig. 13: Acquisition function obtained by Grid Search Algorithm and Bayesian Optimization with sampling over iterations.

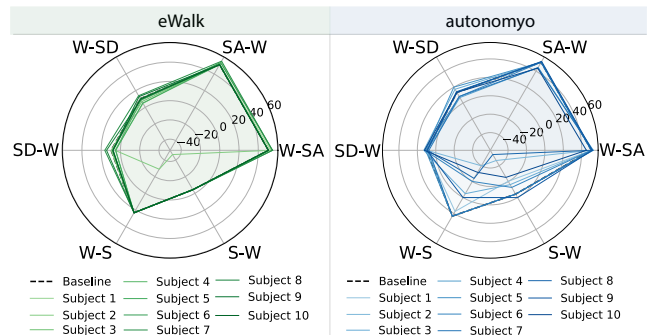


Fig. 14: Changes in the thresholds after BO for each of the transitions for the eWalk and autonomy experiments.

in exoskeleton development [72], [73]. Misalignment, often caused by simplified kinematic models or improper fitting [74], can reduce control accuracy and lead to unwanted interaction forces, negatively impacting user comfort and safety. Given the complexity of human joint mechanics, completely eliminating kinematic mismatches is impractical [72]. Our approach addresses these issues by minimizing the discrepancy between exoskeleton measurements and actual human movement, improving overall system performance.

The learning-based approach presented in this work offers a solution when exoskeleton design cannot be individually adapted, yet reliable kinematic data are still necessary. The remapped joint angles presented in Fig 6 demonstrate improved alignment with natural transitions, such as MHF and HS,

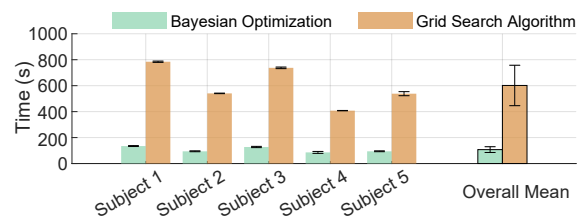


Fig. 15: The computational time for the optimization with BO and GSA for the five subjects.

which are consistent with healthy human biomechanics from the literature [52]. For instance, the $W \rightarrow SD$ transition cycles, despite initial differences, exhibited reduced variance and key features such as MHF and HS that better reflect natural human movement patterns. This is particularly important for the FSM, which relies on these characteristic features for accurate transition detection. Overall, the mapping function validates our approach, supporting the hypothesis that it can generalize across different gait cycles while better capturing natural human movement.

However, the application of the mapping procedure led to mixed results in transition detection accuracy of autonomy experiments. $W \rightarrow S$ and $S \rightarrow W$ transitions showed a 10% decrease in accuracy, while $W \rightarrow SA$ and $SA \rightarrow W$ transitions improved by 10%. Meanwhile, the median accuracy for $W \rightarrow SD$ transitions increased by 20%, with $SA \rightarrow W$ remaining at 100%, as depicted in Fig. 9. Despite some decreases, overall accuracy improved for many subjects, with reduced variability and more consistent performance across different locomotion modes.

These results highlight both the strengths and limitations of the mapping function. While it successfully mitigated human-exoskeleton joint misalignment, slight decreases in $W \rightarrow S$ and $S \rightarrow W$ accuracy point to challenges from user- and system-specific variability, suggesting that performance may vary based on individual physiological characteristics and fit.

Overall, the proposed mapping algorithm effectively addresses joint misalignment, improving joint angle-based locomotion detection and exoskeleton control. Integrating this approach into wearable devices could enhance controller performance, offering more precise, user-specific assistance.

C. The Importance of Personalization

It is well-established in the literature [75], [76], and further confirmed by our research, that individual physiological characteristics and personalized interaction patterns with the exoskeleton significantly influence human-machine interaction. This means that even with high-quality data, users exhibit distinct gait patterns and interaction behaviors, which can affect the exoskeleton's ability to provide optimal assistance. Therefore, it is essential to consider user-specific factors to ensure that the exoskeleton delivers personalized, effective support tailored to the unique needs of each individual.

However, the limited availability of data in the literature, combined with the computational constraints of many exoskeleton systems, often makes it unfeasible to develop deep learning algorithms that generalize effectively across diverse populations while maintaining computational efficiency. Meanwhile, it is well-documented that machine learning models are prone to biases when trained on datasets that lack proper representation of the entire target population [77], [78]. On the other hand, our findings demonstrate that a computationally lightweight FSM, coupled with subject- and system-specific optimization, enhances generalization remarkably improving the accuracy of the transition detection between different locomotion modes.

The results presented in Fig. 10 indicate that while SBA is effective as an initial tuning method for simpler systems like

eWalk, it falls short for more complex systems like autonomy. This limitation arises because SBA is a one-step optimization approach, meaning that only a single set of thresholds can be inferred from the data for a new population. In contrast, BO provides superior performance for both systems, especially for autonomy, which enables a wider range of assistive devices and user variability. The iterative nature of BO allows for continuous refinement of the parameters, which leads to better performance than SBA, especially in complex scenarios.

Given the differences in their effectiveness, we propose a two-step optimization strategy: using SBA for initial threshold tuning, followed by BO to ensure robust performance across varying conditions. As highlighted in Figure 12, the majority of the transitions that needed optimization are effectively handled by BO, which shows robust capability to adapt the FSM even to very specific gait patterns. For example, in the eWalk experiments, Subject 5 showed noteworthy improvements in both $W \rightarrow SD$ and $SD \rightarrow W$ transitions, with accuracy rising from 20% to 100% and from 40% to 100%, respectively. Similarly, Subject 2 had improvements in $W \rightarrow S$ and $S \rightarrow W$ transitions, with accuracies increasing from 80% and 60% to 100% for both transitions and an additional increase from 40% to 80% for the $SA \rightarrow W$ transition.

In the autonomy experiments, BO also yielded substantial gains for Subjects 2 and 6. The accuracy of $W \rightarrow S$ transitions improved from 40% to 100% for Subject 2 and from 60% to 100% for Subject 6. For the $S \rightarrow W$ transitions, accuracies improved from 20% to 100% and from 60% to 100%, respectively for Subjects 2 and 6. Subject 9 in the autonomy experiment also benefited, with $W \rightarrow SD$ accuracy increasing from 20% to 80%, and $SD \rightarrow W$ accuracy improving from 40% to 100%.

The post-optimization thresholds for these transitions, as shown in Fig. 14, diverged notably from their baseline values, suggesting that the optimal thresholds for these subjects were located in distinct regions of the search space. These findings indicate that the gait patterns of these individuals deviated from those of the broader population, underscoring the importance of personalized strategies.

Although the optimization of the thresholds of the FSM algorithm using BO led to substantial improvements in locomotion transition recognition across most of the subjects, for some subjects transition detection accuracy is not as improved as the others as shown in Fig. 12. These challenges likely stem from non-optimized aspects of the FSM, such as the MHF detector or inaccuracies in previously detected transitions, as well as unique subject-specific behaviors that were not fully accounted for during optimization.

For example, in the eWalk experiments, Subject 5s $SA \rightarrow W$ transitions were inaccurately detected due to the timing of MHF detection. This issue was traced back to the MHF detector design rather than the optimization process itself. Specifically, the MHF detector included a velocity range near zero to identify the maximum joint angle in the gait cycle, as the maximum angle occurs when the velocity is close to zero. By expanding this range, we observed improved accuracy but also identified the detector as the root cause of the misclassifications, as shown in Fig. 16-A.

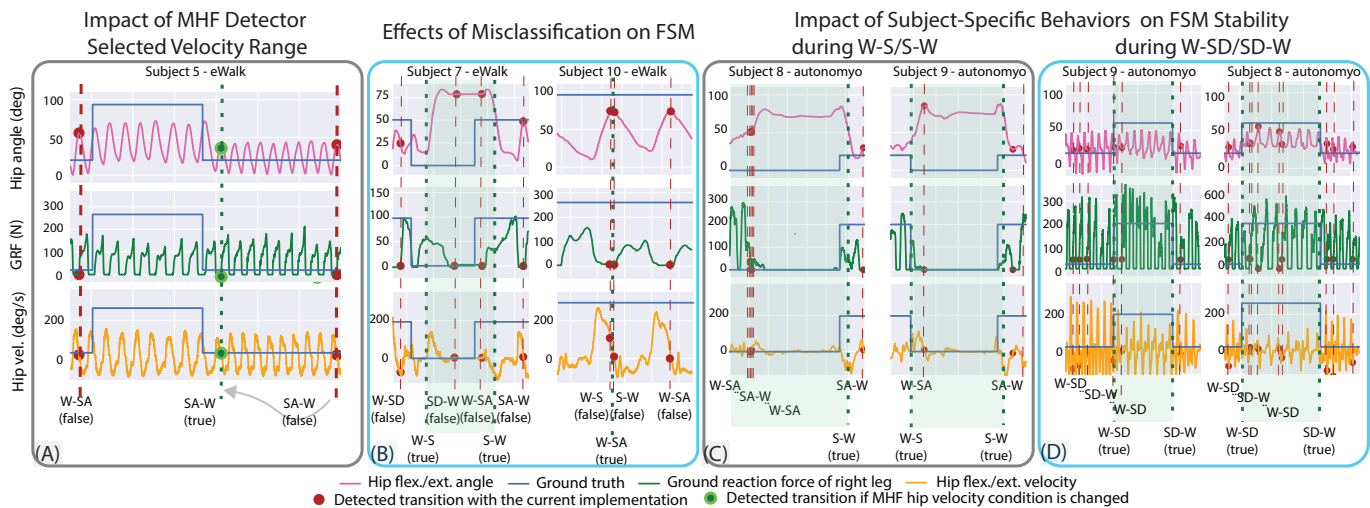


Fig. 16: Investigating the false-detection of the transitions and the underlying reasons with main groups of MHF detector design, previous misclassification, and example of subject-specific patterns.

During Subject 7’s experiments with eWalk, the FSM exhibited instability during $W \rightarrow S$ and $S \rightarrow W$ transitions, prematurely transitioning to SD and preventing the correct detection of the intended transition. This instability could not be resolved by adjusting the $W \rightarrow S/S \rightarrow W$ thresholds alone, as the root cause was linked to the FSMs logic rather than the parameters optimized by BO. Similarly, misclassifications for Subject 10 were traced to the Loaded/Unloaded threshold. The low threshold, combined with signal noise from uncommon movements, led to incorrect transitions, such as detecting $W \rightarrow S$ instead of the intended $W \rightarrow SA$ transition. These two conditions are illustrated in Fig. 16-B.

In the case of Subjects 5, 8, and 9 using the autonomy exoskeleton, the FSM showed notable instability, particularly around the $W \rightarrow SD$ and $SD \rightarrow W$ transitions as depicted for two cases of those subjects in Fig. 16-D. We define instability as when the FSM keeps on switching between two or more classes in consecutive steps, showing confusion and “unstable output” (Fig. 16-C/D). This instability was primarily due to subject-specific behaviors, such as taking small, cautious steps behaviour likely due to discomfort or fear when using the exoskeleton. These small steps caused the FSM to misclassify the transitions, often failing to detect the correct transition sequence, which hindered the optimization process. For instance, Subject 8 not only exhibited instability similar to Subject 5 but also occasionally lifted their leg significantly before descending stairs, leading to further misclassification by triggering SA instead of the intended transition.

Subject 9 encountered a related issue, where the FSM incorrectly identified SA during $W \rightarrow S$ and $S \rightarrow W$ transitions, indicating that no matter the optimization process on $W \rightarrow S/S \rightarrow W$ thresholds, the system would continue to detect SA due to the underlying misclassification tendency as illustrated in Fig. 16-C.

These cases demonstrate that certain behavioral adaptations to the exoskeleton, such as taking small steps or misjudging transitions, cannot be fully mitigated through parameter optimization alone. In cases where the exoskeleton provides

active assistance, the impact of these challenges potentially becomes more significant, as misclassified transitions could result in unintended interaction torques, potentially destabilizing the user or compromising safety. Given that the exoskeleton is intended for individuals with mobility impairments, ensuring a robust response to individual user behaviors is critical for both effectiveness and safety.

To mitigate these risks, the controller for active assistance should be designed to balance responsiveness and stability, aiming to reduce both false positives and false negatives in transition detection. Minimizing false positives is essential to prevent unintentional torques that could disrupt balance while reducing false negatives ensures timely and appropriate assistance during transitions.

This suggests the need for a less restrictive, more adaptable design of exoskeletons to accommodate the variability in user interactions with the exoskeleton. Additionally, training users to interact effectively with the control system could further enhance the safety and intuitiveness of human-machine interaction.

D. The Importance of Real-Time Performance

While personalization and subject-specific optimization are critical for improving exoskeleton performance, these enhancements must be balanced with the computational demands of real-time systems. In our previous study, we demonstrated that an ML-trained TH-based implementation outperforms a rule-based ML classifier in real-time performance on embedded systems used in exoskeletons [2]. More advanced approaches, such as deep learning algorithms, require significantly more computational resources compared to classical event-based state machines. Embedded platforms like the NVIDIA Jetson Xavier can run deep neural networks in real-time [79], but they are still constrained by the maximum sampling rate when used with low-level controllers for transition detection promptly [80].

Given these constraints, event-based state machines offer a computationally efficient alternative for transition detection

algorithms in resource-limited environments. Real-time tuning of thresholds fits well within this framework, prompting us to propose a statistical-based approach and BO for optimization. Although the SBA requires an initial testing period and the involvement of an experienced individual for tuning, it can be integrated into the algorithm to suggest threshold adjustments, providing a pathway for further automation and user-friendly optimization.

BO, while more computationally intensive, eliminates the need for expert tuning or user input. Fig. 15 shows that BO operates four times faster than the GSA. Indeed, as demonstrated in Section V-D, our research demonstrates that high performance can be achieved with low computational cost using adaptive algorithms. For instance, BO took an average of 2 minutes on a personal computer. Even with the limited computational power of an embedded system, subject-specific optimization and supervised testing could suggest new thresholds and improve performance within several minutes.

E. Limitations & Future Work

This study has some limitations that should be acknowledged. A primary limitation of this study is the absence of active assistance in the exoskeletons used during testing. The exoskeletons did not apply assistive torques, meaning user kinematics were unaffected by externally applied torques. When active assistance is enabled, the dynamics of user movement and the associated transition detection may change, potentially increasing false positives or negatives in transition detection. Future research should investigate how assistive torques affect user movement patterns, with particular attention to tuning the FSM parameters to accommodate the changes in gait transitions brought about by assisted movement.

Further limitations include the optimization process, which only focuses on threshold parameters within the FSM. Comprehensive optimization of selected parameters for characteristic moments of FSM could potentially enhance the overall system performance. Additionally, although the sample-efficient method of BO shows promise, we did not implement HIL optimization in real-time. Further refinement will be necessary to enable larger-scale parameter optimization within the FSM in real-time applications.

Moreover, the current method relies on measurements from the right leg during transitions between walking modes. This could lead to misclassifications if a participant primarily uses the left leg during transitions. To improve robustness, future work should include measurements from both legs to enhance the devices versatility and accuracy.

Additionally, the tests were conducted with subjects who had no prior knowledge of the recognition methodology. However, the explainability of the algorithm makes it easily understandable in real-time. We anticipate even better performance if subjects are trained to interact with the algorithm, and future research will explore this aspect to improve human-machine interaction.

Ultimately, we recognize the importance of studying diverse populations to ensure the systems effectiveness and safety for a broader user base. Therefore, our next study will

aim to include participants with varying characteristics and mobility impairments, enabling us to evaluate the systems performance across different user profiles.

VII. CONCLUSION

This study introduced two methods, the Statistics-Based Approach and Bayesian Optimization, to personalize transition detection thresholds of the utilized FSM for lower-limb exoskeletons. Additionally, we addressed joint misalignment issues commonly encountered in human-exoskeleton interactions. Human subject experiments conducted with two distinct exoskeletons, eWalk, and autonomy, demonstrated the effectiveness of these approaches in accurately detecting transitions between locomotion modes. Mitigating joint misalignment and optimizing FSM thresholds allowed the system to adapt to individual gait patterns and system-specific characteristics, resulting in reliable performance across a diverse user base.

Our results underscore the potential of these methods for practical applications in assistive devices, where subject- and system-specific adaptation is critical for enhancing transition detection performance. To support future research, we also provided an open-source dataset of lower-limb kinematics from 18 subjects in total with two exoskeletons, offering a valuable resource for further development in locomotion mode detection and control strategies.

ACKNOWLEDGMENT

We thank Salim Bousofara for his valuable contribution to the preparation of the dataset and the accompanying scripts. We thank FAULHABER SA and Sonceboz for their support for the development of the exoskeletons. We thank all the subjects who voluntarily participated in the experiments. We thank the vector drawings designed by stories/Freepik that have been used in Figs.1 and 2.

REFERENCES

- [1] S. Cheng, E. Bolivar-Nieto, and R. D. Gregg, "Real-time activity recognition with instantaneous characteristic features of thigh kinematics," *IEEE TNSRE*, vol. 29, pp. 1827–1837, 2021.
- [2] Z. . Orhan, A. Dal Prete, A. Bolotnikova, M. Gandolla, A. Ijspeert, and M. Bouri, "Real-time locomotion transitions detection: Maximizing performances with minimal resources," in *IEEE ICRA*, 2024, pp. 3241–3247.
- [3] R. Kolaghassi, M. K. Al-Hares, and K. Sirlantzis, "Systematic review of intelligent algorithms in gait analysis and prediction for lower limb robotic systems," *IEEE Access*, vol. 9, pp. 113 788–113 812, 2021.
- [4] R. Gehlhar, M. Tucker, A. J. Young, and A. D. Ames, "A review of current state-of-the-art control methods for lower-limb powered prostheses," *Annual Reviews in Control*, vol. 55, pp. 142–164, 2023.
- [5] D. Wang, X. Gu, and H. Yu, "Sensors and algorithms for locomotion intention detection of lower limb exoskeletons," *Medical Engineering and Physics*, vol. 113, no. February, p. 103960, 2023.
- [6] H. Allahbakhshi, T. Hinrichs, H. Huang, and R. Weibel, "The Key Factors in Physical Activity Type Detection Using Real-Life Data: A Systematic Review," *Frontiers in Physiology*, vol. 10, pp. 1–20, 2019.
- [7] A. H. Al-dabbagh and R. Ronsse, "A review of terrain detection systems for applications in locomotion assistance," *Robotics and Autonomous Systems*, vol. 133, 2020.
- [8] X. Zhang, E. Tricomi, F. Missiroli, N. Lotti, and L. Masia, "Real-time assistive control via imu locomotion mode detection in a soft exosuit: An effective approach to enhance walking metabolic efficiency," *IEEE/ASME Transactions on Mechatronics*, vol. 29, no. 3, pp. 1797–1808, 2024.

- [9] S. J. Preece, J. Y. Goulermas, L. P. J. Kenney, D. Howard, K. Meijer, and R. Crompton, "Activity identification using body-mounted sensors: a review of classification techniques," *Physiological Measurement*, vol. 30, no. 4, pp. R1–R33, 2009.
- [10] M. Pesenti, G. Invernizzi, J. Mazzella, M. Boccione, A. Pedrocchi, and M. Gandolla, "Imu-based human activity recognition and payload classification for low-back exoskeletons," *Scientific Reports*, vol. 13, no. 1, p. 1184, 2023.
- [11] F. Attal, S. Mohammed, M. Dedabrishvili, F. Chamroukhi, L. Oukhellou, and Y. Amirat, "Physical Human Activity Recognition Using Wearable Sensors," *Sensors*, vol. 15, no. 12, pp. 3134–3138, 2015.
- [12] J. Pohl, A. Ryser, J. M. Veerbeek, G. Verheyden, J. E. Vogt, A. R. Luft, and C. A. Easthope, "Accuracy of gait and posture classification using movement sensors in individuals with mobility impairment after stroke," *Frontiers in Physiology*, vol. 13, no. September, pp. 1–14, 2022.
- [13] K. Yuan, Q. Wang, and L. Wang, "Fuzzy-logic-based terrain identification with multisensor fusion for transtibial amputees," *IEEE/ASME Transactions on Mechatronics*, vol. 20, no. 2, pp. 618–630, 2015.
- [14] A. Narayan, F. A. Reyes, M. Ren, and Y. Haoyong, "Real-Time Hierarchical Classification of Time Series Data for Locomotion Mode Detection," *IEEE Journal of Biomedical and Health Informatics*, vol. 26, no. 4, pp. 1749–1760, 2022.
- [15] J. Lobo-Prat, P. N. Kooren, A. H. A. Stienen, J. L. Herder, B. F. J. M. Koopman, and P. H. Veltink, "Non-invasive control interfaces for intention detection in active movement-assistive devices," *Journal of neuroengineering and rehabilitation*, vol. 11, no. 1, p. 168, 2014.
- [16] I. Kang, D. D. Molinaro, G. Choi, and A. J. Young, "Continuous locomotion mode classification using a robotic hip exoskeleton," in *IEEE BioRob*. IEEE, 2020, pp. 376–381.
- [17] S. R. Donahue and M. E. Hahn, "Feature Identification With a Heuristic Algorithm and an Unsupervised Machine Learning Algorithm for Prior Knowledge of Gait Events," *IEEE TNSRE*, vol. 30, pp. 108–114, 2022.
- [18] Y. Qian, Y. Wang, C. Chen, J. Xiong, Y. Leng, H. Yu, and C. Fu, "Predictive locomotion mode recognition and accurate gait phase estimation for hip exoskeleton on various terrains," *IEEE RA-L*, vol. 7, no. 3, pp. 6439–6446, 2022.
- [19] M. R. Haque, M. R. Islam, E. Sazonov, and X. Shen, "Swing-phase detection of locomotive mode transitions for smooth multi-functional robotic lower-limb prosthesis control," *Frontiers in Robotics and AI*, vol. 11, 2024.
- [20] Z. Wang, J. Pang, P. Tao, Z. Ji, J. Chen, L. Meng, R. Xu, and D. Ming, "Locomotion transition prediction at anticipatory locomotor adjustment phase with shap feature selection," *Biomedical Signal Processing and Control*, vol. 92, p. 106105, 2024.
- [21] S. Cheng, C. A. Laubscher, and R. D. Gregg, "Controlling powered prosthesis kinematics over continuous inter-leg transitions between walking and stair ascent/descent," June 2024. [Online]. Available: <http://dx.doi.org/10.36227/techrxiv.171778818.88300126/v1>
- [22] Z. Zhou, X. Liu, Y. Jiang, J. Mai, and Q. Wang, "Real-time onboard SVM-based human locomotion recognition for a bionic knee exoskeleton on different terrains," in *Wearable Robotics Association Conference (WearRAcon)*. IEEE, 2019, pp. 34–39.
- [23] Z. Lu, A. Narayan, and H. Yu, "A deep learning based end-to-end locomotion mode detection method for lower limb wearable robot control," in *IEEE IROS*, 2020, pp. 4091–4097.
- [24] H. T. T. Vu, H.-L. Cao, D. Dong, T. Verstraten, J. Geeroms, and B. Vanderborght, "Comparison of machine learning and deep learning-based methods for locomotion mode recognition using a single inertial measurement unit," *Frontiers in Neurorobotics*, vol. 16, 2022.
- [25] H. Eken, F. Lanotte, V. Papapicco, M. F. Penna, E. Gruppioni, E. Trigili, S. Crea, and N. Vitiello, "A locomotion mode recognition algorithm using adaptive dynamic movement primitives," *IEEE TNSRE*, vol. 31, pp. 4318–4328, 2023.
- [26] F. Labarrière, E. Thomas, L. Calistri, V. Optasanu, M. Gueugnon, P. Ornetti, and D. Laroche, "Machine Learning Approaches for Activity Recognition and/or Activity Prediction in Locomotion Assistive Devices: A Systematic Review," *Sensors*, vol. 20, no. 21, p. 6345, 2020.
- [27] A. Young, A. Simon, N. Fey, and L. Hargrove, "Intent recognition in a powered lower limb prosthesis using time history information," *Annals of Biomedical Engineering*, vol. 42, no. 3, pp. 631–641, 2014.
- [28] B. Su, J. Wang, S. Liu, M. Sheng, J. Jiang, and K. Xiang, "A cnn-based method for intent recognition using inertial measurement units and intelligent lower limb prosthesis," *IEEE TNSRE*, vol. 27, pp. 1032–1042, 2019.
- [29] L. Moreira, J. Figueiredo, J. Cerqueira, and C. P. Santos, "A Review on Locomotion Mode Recognition and Prediction When Using Active Orthoses and Exoskeletons," *Sensors*, vol. 22, no. 19, p. 7109, 2022.
- [30] Y. Long, Z.-J. Du, W.-D. Wang, G.-Y. Zhao, G.-Q. Xu, L. He, X.-W. Mao, and W. Dong, "Pso-svm-based online locomotion mode identification for rehabilitation robotic exoskeletons," *Sensors*, vol. 16, no. 9, 2016.
- [31] C. Wang, X. Wu, Y. Ma, G. Wu, and Y. Luo, "A Flexible Lower Extremity Exoskeleton Robot with Deep Locomotion Mode Identification," *Complexity*, vol. 2018, pp. 1–9, 2018.
- [32] X. Liu and Q. Wang, "Real-Time Locomotion Mode Recognition and Assistive Torque Control for Unilateral Knee Exoskeleton on Different Terrains," *IEEE/ASME Transactions on Mechatronics*, vol. 25, no. 6, pp. 2722–2732, 2020.
- [33] G. Du, J. Zeng, C. Gong, and E. Zheng, "Locomotion Mode Recognition with Inertial Signals for Hip Joint Exoskeleton," *Applied Bionics and Biomechanics*, vol. 2021, pp. 1–11, 2021.
- [34] I. Kang, D. D. Molinaro, G. Choi, J. Camargo, and A. J. Young, "Subject-Independent Continuous Locomotion Mode Classification for Robotic Hip Exoskeleton Applications," *IEEE Transactions on Biomedical Engineering*, vol. 69, no. 10, pp. 3234–3242, 2022.
- [35] L. Alzubaidi, J. Bai, A. Al-Sabaawi, J. Santamara, A. S. Albahri, B. S. N. Al-dabbagh, M. A. Fadhel, M. Manoufali, J. Zhang, A. H. Al-Timemy, Y. Duan, A. Abdullah, L. Farhan, Y. Lu, A. Gupta, F. Albu, A. Abbosh, and Y. Gu, "A survey on deep learning tools dealing with data scarcity: definitions, challenges, solutions, tips, and applications," *Journal of Big Data*, vol. 10, no. 1, p. 46, 2023.
- [36] R. E. Quesada, J. M. Caputo, and S. H. Collins, "Increasing ankle push-off work with a powered prosthesis does not necessarily reduce metabolic rate for transtibial amputees," *Journal of Biomechanics*, vol. 49, no. 14, pp. 3452–3459, 2016.
- [37] M. Kim, Y. Ding, P. Malcolm, J. Speeckaert, C. J. Siviyy, C. J. Walsh, and S. Kuindersma, "Human-in-the-loop bayesian optimization of wearable device parameters," *PLOS ONE*, vol. 12, no. 9, pp. 1–15, 09 2017.
- [38] P. Slade, C. Atkeson, J. M. Donelan, H. Houdijk, K. A. Ingraham, M. Kim, K. Kong, K. L. Poggensee, R. Riener, M. Steinert, J. Zhang, and S. H. Collins, "On human-in-the-loop optimization of humanrobot interaction," *Nature*, vol. 633, no. 8031, pp. 779–788, sep 2024.
- [39] J. Zhang, P. Fiers, K. A. Witte, R. W. Jackson, K. L. Poggensee, C. G. Atkeson, and S. H. Collins, "Human-in-the-loop optimization of exoskeleton assistance during walking," *Science*, vol. 356, no. 6344, pp. 1280–1284, 2017.
- [40] Y. Ding, M. Kim, S. Kuindersma, and C. J. Walsh, "Human-in-the-loop optimization of hip assistance with a soft exosuit during walking," *Science Robotics*, vol. 3, no. 15, p. eaar5438, 2018.
- [41] L. Xu, X. Liu, Y. Chen, L. Yu, Z. Yan, C. Yang, C. Zhou, and W. Yang, "Reducing the muscle activity of walking using a portable hip exoskeleton based on human-in-the-loop optimization," *Frontiers in Bioengineering and Biotechnology*, vol. 11, 2023.
- [42] E. Brochu, V. M. Cora, and N. de Freitas, "A tutorial on bayesian optimization of expensive cost functions, with application to active user modeling and hierarchical reinforcement learning," *CoRR*, vol. abs/1012.2599, 2010. [Online]. Available: <http://arxiv.org/abs/1012.2599>
- [43] J. Snoek, H. Larochelle, and R. P. Adams, "Practical bayesian optimization of machine learning algorithms," in *Advances in Neural Information Processing Systems*, F. Pereira, C. Burges, L. Bottou, and K. Weinberger, Eds., vol. 25. Curran Associates, Inc., 2012.
- [44] T.-C. Wen, M. Jacobson, X. Zhou, H.-J. Chung, and M. Kim, "The personalization of stiffness for an ankle-foot prosthesis emulator using human-in-the-loop optimization," in *IEEE/RJS IROS*, 2020, pp. 3431–3436.
- [45] A. Reiss, "PAMAP2 Physical Activity Monitoring," UCI Machine Learning Repository, 2012.
- [46] M. Zhang and A. A. Sawchuk, "Usc-had: A daily activity dataset for ubiquitous activity recognition using wearable sensors," in *Proceedings of the ACM Conference on Ubiquitous Computing*, ser. UbiComp '12. New York, NY, USA: Association for Computing Machinery, 2012, p. 10361043.
- [47] C. A. Fukuchi, R. Fukuchi, and M. Duarte, "A public dataset of overground and treadmill walking kinematics and kinetics in healthy individuals," *PeerJ*, vol. 6, p. e4640, 2018.
- [48] S. Khandelwal and N. Wickstrm, "Evaluation of the performance of accelerometer-based gait event detection algorithms in different real-world scenarios using the marea gait database," *Gait and Posture*, vol. 51, pp. 84–90, 2017.
- [49] R. Chereshevnev and A. Kertesz-Farkas, "Hugadb: Human gait database for activity recognition from wearable inertial sensor networks," in *International Conference on Analysis of Images, Social Networks and Texts*. Springer, 2017, pp. 131–141.

- [50] F. Horst, D. Slijepcevic, M. Simak, and W. I. Schllhorn, "Gutenberg gait database, a ground reaction force database of level overground walking in healthy individuals," *Sci Data*, vol. 8, no. 1, p. 232, 2021.
- [51] Y. Luo, S. M. Coppola, P. C. Dixon, S. Li, J. T. Dennerlein, and B. Hu, "A database of human gait performance on irregular and uneven surfaces collected by wearable sensors," *Scientific Data*, vol. 7, no. 1, p. 219, 2020.
- [52] E. Reznick, K. R. Embry, R. Neuman, E. Bolivar-Nieto, and R. D. Gregg, "Lower-limb kinematics and kinetics during continuously varying human locomotion," *Nature, Scientific Data*, vol. 8, 2021.
- [53] F. Pedregosa et al, "Scikit-learn: Machine learning in python," *JMLR* 12, pp., 2011.
- [54] S. Messara, A. R. Manzoori, A. Di Russo, A. Ijspeert, and M. Bouri, "Novel design and implementation of a neuromuscular controller on a hip exoskeleton for partial gait assistance," in *IEEE ICORR*, 2023, pp. 1–6.
- [55] A. R. Manzoori, D. Malatesta, A. Mortier, et al., "Adaptive hip exoskeleton control using heart rate feedback reduces oxygen cost during ecological locomotion," *Research Square*, June 2024, pREPRINT (Version 1).
- [56] A. Ortlieb, M. Bouri, R. Baud, and H. Bleuler, "An assistive lower limb exoskeleton for people with neurological gait disorders," in *IEEE ICORR*, 2017, pp. 441–446.
- [57] Z. . Orhan, M. Shafiee, V. Juillard, J. C. Oliveira, A. Ijspeert, and M. Bouri, "Exorecovery: Push recovery with a lower-limb exoskeleton based on stepping strategy," in *IEEE ICRA*, 2024, pp. 3248–3255.
- [58] A. Schiele and F. C. van der Helm, "Kinematic design to improve ergonomics in human machine interaction," *IEEE TNSRE : a publication of the IEEE Engineering in Medicine and Biology Society*, vol. 14(4), pp. 456–469, 2006.
- [59] A. Stienen, E. Hekman, F. van der Helm, and H. Kooij, "Self-aligning exoskeleton axes through decoupling of joint rotations and translations," *Robotics, IEEE Transactions on*, vol. 25, pp. 628 – 633, 07 2009.
- [60] B. Celebi, M. Yalcin, and V. Patoglu, "Assiston-knee: A self-aligning knee exoskeleton," in *IEEE IROS*, 2013, pp. 996–1002.
- [61] M. Givvez and A. Aceves-Lopez, "A review on compliant joint mechanisms for lower limb exoskeletons," *Journal of Robotics*, 2016.
- [62] C. M. Bishop, *Pattern Recognition and Machine Learning (Information Science and Statistics)*. Berlin, Heidelberg: Springer-Verlag, 2006.
- [63] R. Garnett, *Bayesian Optimization*. Cambridge University Press, 2023.
- [64] GPpy, "GPpy: A gaussian process framework in python," <http://github.com/SheffieldML/GPpy>, since 2012.
- [65] C. E. Rasmussen and C. K. I. Williams, *Gaussian Processes for Machine Learning*. The MIT Press, 2006.
- [66] I. Goodfellow, Y. Bengio, and A. Courville, *Deep Learning*. MIT Press, 2016.
- [67] F. Chollet, *Deep Learning with Python, Second Edition*. Manning, 2021.
- [68] "Exomove - biomechanical dataset of daily activities with lower-limb exoskeletons," <https://zenodo.org/records/14076104>, accessed: 2024-11-14.
- [69] J. K. Moore, S. K. Hnat, and A. J. van den Bogert, "An elaborate data set on human gait and the effect of mechanical perturbations," *PeerJ*, vol. 3, p. e918, 2015.
- [70] B. Hu, E. Rouse, and L. Hargrove, "Benchmark datasets for bilateral lower-limb neuromechanical signals from wearable sensors during unassisted locomotion in able-bodied individuals," *Frontiers in Robotics and AI*, vol. 5, p. 14, 2018.
- [71] J. Camargo, A. Ramanathan, W. Flanagan, and A. J. Young, "A comprehensive open-source dataset of lower limb biomechanics in multiple conditions of stairs, ramps, and level-ground ambulation and transitions," *Elsevier, Journal of Biomechanics*, vol. 119, 2021.
- [72] M. B. Nf, K. Junius, M. Rossini, C. Rodriguez-Guerrero, B. Vanderborght, and D. Lefeber, "Misalignment Compensation for Full Human-Exoskeleton Kinematic Compatibility: State of the Art and Evaluation," *Applied Mechanics Reviews*, vol. 70, no. 5, p. 050802, 02 2019.
- [73] C. Siviý, L. M. Baker, B. T. Quinlivan, F. Porciuncula, K. Swaminathan, L. N. Awad, and C. J. Walsh, "Opportunities and challenges in the development of exoskeletons for locomotor assistance," *Nature Biomedical Engineering*, vol. 7, no. 4, pp. 456–472, 2023.
- [74] J. Bessler-Etten, L. Schaake, G. B. Prange-Lasonder, and J. H. Buurke, "Assessing effects of exoskeleton misalignment on knee joint load during swing using an instrumented leg simulator," *Journal of NeuroEngineering and Rehabilitation*, vol. 19, no. 1, p. 13, 2022.
- [75] G. L. Kirkwood, C. D. Otmar, and M. Hansia, "Who's leading this dance?: Theorizing automatic and strategic synchrony in human-exoskeleton interactions," *Frontiers in Psychology*, vol. 12, 2021.
- [76] S. Massardi, D. Rodriguez-Cianca, D. Pinto-Fernandez, J. C. Moreno, M. Lancini, and D. Torricelli, "Characterization and evaluation of

humanexoskeleton interaction dynamics: A review," *Sensors*, vol. 22, no. 11, 2022.

- [77] N. Mehrabi, F. Morstatter, N. Saxena, K. Lerman, and A. Galstyan, "A survey on bias and fairness in machine learning," 2022. [Online]. Available: <https://arxiv.org/abs/1908.09635>
- [78] T. Hellström, V. Dignum, and S. Bensch, "Bias in machine learning – what is it good for?" 2020. [Online]. Available: <https://arxiv.org/abs/2004.00686>
- [79] M. Vandersteegen, K. V. Beeck, and T. Goedemé, "Super accurate low latency object detection on a surveillance uav," *International Conference on Machine Vision Applications*, pp. 1–6, 2019.
- [80] H. Lu, L. R. Schomaker, and R. Carloni, "Imu-based deep neural networks for locomotor intention prediction," in *IEEE IROS*, 2020, pp. 4134–4139.



Andrea Dal Prete received his B.S. degree in Mechanical Engineering in 2021 and his M.S. degree in Mechatronics Engineering in 2023, from Politecnico di Milano, Italy. Currently, he is a Ph.D. candidate in Mechanical Engineering at Politecnico di Milano. His research focuses on bioinspired and intelligent robotics and motor assistance for industrial activities, particularly for workers performing exhausting tasks.



Zeynep zge Orhan received her B.S. degree in Mechanical Engineering from METU, Turkey, in 2017, and her M.S. degree in Mechatronics Engineering from Sabanci University, Turkey, in 2020. She is currently a Ph.D. candidate at EPFL. Her research focuses on developing assistive control strategies for lower-limb exoskeletons to assist daily living activities.



Anastasia Bolotnikova received her M.Sc. degree in Computer Science from the University of Tartu, Estonia, in 2017 and her Ph.D. in Robotics at the University of Montpellier, France, in 2021, then she was a postdoctoral researcher at EPFL. Since 2024, she is a research fellow at the Laboratory for Analysis and Architecture of Systems (LAAS-CNRS). Her research interests include robotic physical assistance and tactile communication.



Marta Gandolla is an Assistant Professor in the Department of Mechanical Engineering at Politecnico di Milano. She received her M.Sc. in Biomedical Engineering in 2009 and her Ph.D. in Bioengineering with European cum laude honors in 2013 from Politecnico di Milano. Her research explores neurological motor rehabilitation and motor assistance, with a focus on daily life activities for fragile individuals and workers in physically demanding tasks.



Auke Ijspeert is a Full Professor at EPFL and head of the Biorobotics Laboratory. He holds a B.Sc. and M.Sc. in Physics from EPFL (1995) and a Ph.D. in Artificial Intelligence from the University of Edinburgh (1999). His research lies at the intersection of robotics, computational neuroscience, nonlinear dynamical systems, and applied machine learning. He also works on assisting people with limited mobility using exoskeletons and assistive furniture.



Mohamed Bouri is the group leader of the REHAssist group at EPFL. He received his degree in Electrical Engineering in 1992 and his Ph.D. in Industrial Automation in 1997 from INSA Lyon, France. Since joining EPFL in 1997, he has been active in robot control, automation, and design for medical and industrial applications. His current research focuses on exoskeleton development and associated control strategies.